Adsorption and Photooxidation of CH_3CN on TiO_2

J. Zhuang, C. N. Rusu, and J. T. Yates, Jr.*

Surface Science Center, Department of Chemistry, University of Pittsburgh, Pittsburgh, Pennsylvania, 15260

Received: March 26, 1999; In Final Form: June 15, 1999

The adsorption and photooxidation of CH_3CN chemisorbed on TiO_2 has been investigated using infrared spectroscopy. It was found that CH_3CN forms an ice layer on TiO_2 at 126K and above 126K CH_3CN diffusion into TiO_2 occurs. At 200K, the adsorption of CH_3CN on both isolated Ti−OH groups and on the Ti^{4+} Lewis acid site was observed. Under UV irradiation (350 ± 50 nm; hυ = 3.10−4.13 eV), CH_3CN was oxidized in the presence of O_2 to form H_2O, CO_2, surface CO_3^{2-} and an intermediate partially oxidized isocyanate species, NCO, which was identified by various isotopic experiments. Photooxidation of the CH_3 moiety in adsorbed CH_3CN occurs more readily does the CN moiety in CH_3CN. Lattice oxygen of TiO_2 was found to preferentially form adsorbed NCO, compared to oxygen from adsorbed O_2. A mechanism of the formation of NCO species was postulated.

I. Introduction

TiO_2 has been extensively used in the field of heterogeneous photooxidation catalysis for environmental cleanup because TiO_2 is nontoxic, stable, and inexpensive. Band gap excitation can occur from the UV end of the solar spectrum.[1−4] Many organic molecules such as trichloroethylene(TCE),[5−7] 4-chlorophenol-(4-CP)[8] and CH_3Cl[9] have been effectively oxidized on the TiO_2 surface into small inorganic molecules under UV irradiation. It is well-known that electron−hole pairs are generated when TiO_2 is irradiated by UV photons with energy higher than the TiO_2 band gap energy (3.2 eV) and these excitons can migrate to the TiO_2 surface to initiate redox reactions with adsorbates. The mechanism of photooxidation on TiO_2 surfaces is still under discussion.

It is proposed that surface hydroxyl groups react with the holes and form •OH radicals, which then oxidize the surface absorbates.[10−12] Support for this mechanism comes from the chemical identification of the hydroxylated oxidation intermediates,[13−16] EPR detection of surface •OH radical in aqueous TiO_2 sols,[17−18] the use of •OH radical scavengers[19] and the kinetic isotope effect.[20] Preadsorbed oxygen is believed to trap the electron to prevent the recombination of the electron−hole pairs, increasing the lifetime of the hole states.[2−3] However, degradation of 4-CP studied by Stafford et al. shows that oxygen is not only just an electron scavenger but also participates in the oxidation reaction.[8] In another study the presence of adsorbed molecular oxygen was proven to be essential in the photooxidation of CH_3Cl.[21] In addition, Fan and Yates found in the photooxidation of TCE that the surface hydroxyl groups are not consumed, which implies that surface hydroxyl groups are not involved in this process.[22] Okamoto et al. suggests that hydroxyl radical can be formed via photoelectrons and oxygen. The $O_2^{\bullet -}$ from the reaction of a photoelectron and O_2 reacts with H^+ to form $HO_2^{\bullet}$ which produces H_2O_2. The H_2O_2 molecule then produces 2 •OH species under UV irradiation.[23]

Acetonitrile has been widely used as a probe molecule to characterize the surface states of various metal oxides since the frequency of the CN stretching mode is sensitive to the bonding site for the molecule.[24−27] Due to the nitrogen electron lone pair, υ(CN) increases when electron donor−acceptor complexes are formed between CH_3CN and the surface. From the extent of the increase of υ(CN), sites with different acidity can be identified. Infrared studies of CH_3CN adsorption on zeolites clearly showed that different adsorbing sites of zeolites can be effectively distinguished.[26] The relative surface acid strength of ZnO, Al_2O_3, and alumina-pillared montmorillonite (ALPM) was measured using acetonitrile as a probe molecule.[28] Early studies of the adsorption of CH_3CN on Al_2O_3 explicitly showed the existence of Lewis and Brønsted acid sites on the surface.[29]

Acetonitrile is an interesting molecule for photooxidation studies. It possesses both an alkyl and a cyanide carbon atom which may undergo different oxidation routes. In addition, the CN moiety is representative of a number of toxic materials which are candidates for TiO_2-based solar driven photooxidation processes. Despite the interest in CH_3CN as a model adsorbate, only one study of its photooxidation on TiO_2 is known to us. Lichtin et al. described the photocatalyzed oxidative degradation of CH_3CN on TiO_2.[30] They found that the final products of the photooxidation of CH_3CN were CO_2, H_2O, and HNO_3. The $(CN)_2$ species was identified as an intermediate by gas chromatography.

In this study, the adsorption and photooxidation of CH_3CN was examined on powdered TiO_2 by transmission infrared spectroscopy. The frequency of the υ(CN) mode was found to be very helpful for determining aspects of the mechanism of photooxidation of CH_3CN on TiO_2. The high-surface-area powdered TiO_2, possessing several different kinds of crystallographic planes and defects, provides important insight about the photooxidation of CH_3CN on technologically useful TiO_2 photocatalysts.

II. Experimental Section

Experiments were carried out in a bakeable stainless steel IR cell capable of operating with a sample temperature from 100K to 1500K. A detailed description of the IR cell had been reported previously[31] and its use in photochemistry experiments has also been described.[21] TiO_2 powder was pressed into a tungsten grid which was then fastened in the cell rigidly using a pair of nickel clamps. A K-type thermocouple was spot-welded on the top-central region of the tungsten grid to measure the

10.1021/jp991040w CCC: $18.00
Published on Web 08/03/1999

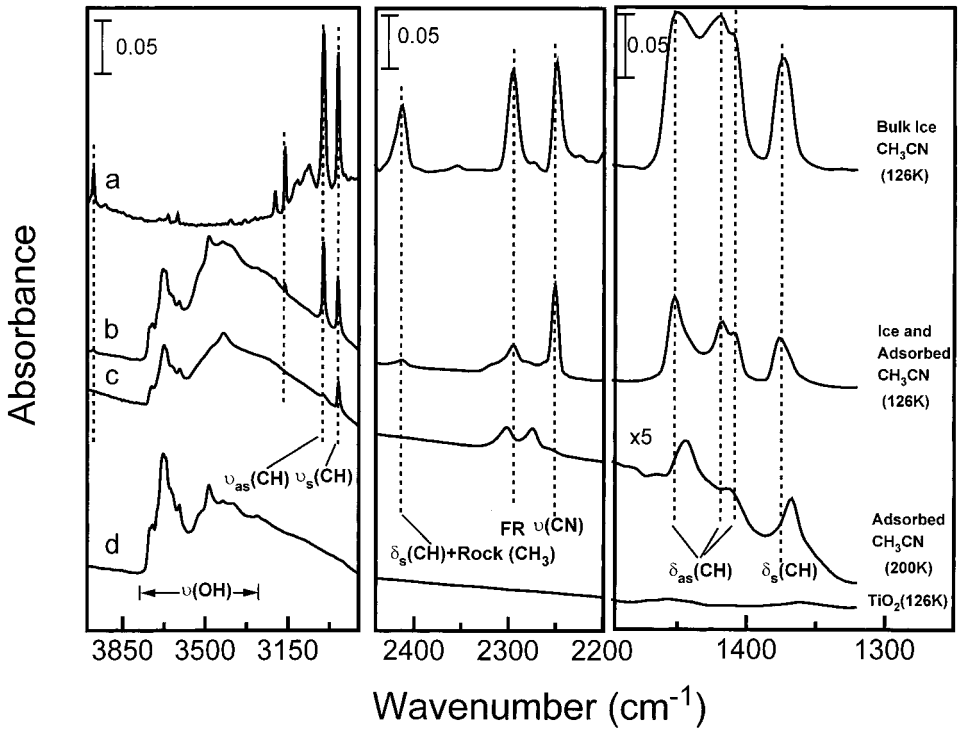

Figure 1. The IR spectra of condensed and adsorbed CH_3CN on TiO_2 at 126 K and 200 K showing the ice multilayer and chemisorbed layer of CH_3CN.

TABLE 1: Comparison of IR Vibrational Frequencies of Different States of CH_3CN

	frequency (cm^{-1})						
states	υ_{as}(CH)	υ_s(CH)	FR[a]	υ(CN)	δ_{as}(CH)	δ_s(CH)	reference
CH_3CN (s,126K)	3001	2939	2295	2251	1452 1417 1408	1377	this work
CH_3CN (a,200K) (on TiO_2)	3001	2939	2303	2274	1444 1414	1367	this work
CH_3CN (s, 81K)	2996	2933	2293	2247	1436 1425 1421 1419	1370 1368 1366	33
CH_3CN (s,208K)	3000	2936	2294	2249	1430 1420	1370 1368	33
CH_3CN (l,238K)	3001	2942	2293	2252	1415	1374	33
CH_3CN (g,300K)	3009	2954	2305	2268	1454	1389	34

[a] FR represents the Fermi resonance mode of υ(CN).

temperature of the sample. The sample temperature could be easily adjusted using liquid nitrogen and electrical heating of the grid via a programmable controller.[32] The TiO_2 sample was pressed only on one-half of the tungsten grid while the other half of the grid had no sample. Therefore the infrared spectra of the TiO_2 surface and of the gaseous species (through the empty half grid) could be measured alternatively.

The IR cell was connected to a stainless steel vacuum system pumped by both turbomolecular and ion pumps and the base pressure was better than 1×10^{-8} Torr. The pressure was measured by a capacitance manometer (Baratron, 116A, MKS, range $10^{-3}-10^{3}$ Torr) or the ion current drawn by the ion pump (Varian, 921−0062). Infrared spectra were obtained with a nitrogen gas purged Mattson Fourier transform infrared spectrometer (Research Series 1) equipped with a wide band HgCdTe detector operating at 77K. The sample spectra shown here were recorded with 4 cm^{-1} resolution using 500 scans while the background spectra were recorded with 4 cm^{-1} resolution using 1000 scans.

The UV source is a 350-W high-pressure mercury arc lamp (Oriel Corp.) with a 350 ± 50 nm band-pass filter. A manual shutter was installed to accurately control the UV exposure time. The photon flux at 350 nm is 1.7×10^{15} photons cm^{-2} s^{-1} in our measurement using a thermopile (2M type). The TiO_2 powder on the tungsten grid was positioned in such a way that both the IR beam from the FTIR spectrometer and the UV light from the mercury arc lamp are focused on it at an angle of incidence of about 45° to the normal of the grid. The orthogonal arrangement of UV light with the IR beam makes IR measurements possible during photochemistry on the surface.

The TiO_2 used was Degussa titanium dioxide P25 which is reported to have 70% anatase and 30% rutile component and a surface area of ~50m^2/g. Before any experiment, the TiO_2 was pretreated in a 6 Torr O_2 atmosphere at 673K for 15 min to remove traces of organic contamination. After that, the TiO_2 was reduced or oxidized for different experiments. The optical density of the TiO_2 was 4.7 mg/cm^2 of open grid area.

The oxygen gas was obtained from Matheson Gas Products with 99.998% purity. The $^{18}O_2$ gas was obtained from ICON Services Inc. with an isotopic purity of 95 atom %. The acetonitrile was purchased from Aldrich with a purity of 99+%. The isotopic acetonitrile samples (CD_3CN, $CH_3C^{15}N$ and $CH_3{}^{13}CN$) were purchased from Cambridge Isotope Laboratories with a purity of 99.8%, 98+%, and 99% respectively. All samples of acetonitrile were further purified with several freeze−pump−thaw cycles using liquid nitrogen before their use. Ultrapure H_2O was prepared by ion-exchange and distillation and then purged by nitrogen gas for 30 min to remove dissolved CO_2 gas.

III. Results

1. Low-Temperature Adsorption of CH_3CN on TiO_2. Figure 1 shows the FTIR spectra of condensed and adsorbed

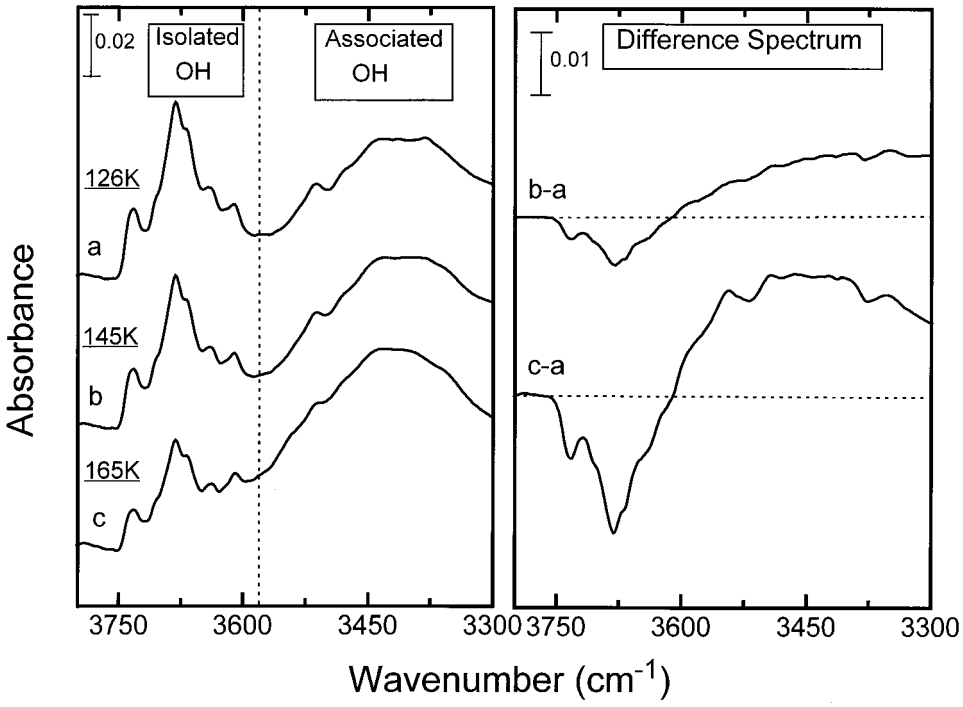

Figure 2. IR spectra in the υ(OH) region for adsorption of CH_3CN on TiO_2 showing the effect of CH_3CN diffusion on TiO_2 with increasing temperature.

CH_3CN on TiO_2 at 126K and 200K. The contribution from gaseous species was negligible in all of the FTIR spectra of Figure 1 because spectra were recorded under vacuum. Figure 1a shows a reference spectrum of the bulk ice CH_3CN layer which was obtained by condensing a very large amount of CH_3CN onto the surface of the TiO_2. The surface OH features on the TiO_2 were eliminated due to an optical screening effect of the thick CH_3CN layer. Two IR bands at 3001 and 2939 cm^{-1} are assigned to the asymmetric and symmetric CH_3 stretching modes, respectively. The 2251 and 2295 cm^{-1} bands are due to the CN stretching mode and its Fermi resonance mode. The 1452, 1417, and 1408 cm^{-1} bands are believed to be the asymmetric CH deformation modes and the 1377 cm^{-1} band is the symmetric CH deformation mode. Figure 1b and 1c show the spectra of a much lower coverage of CH_3CN adsorbed on TiO_2 at 126K and 200K, respectively. It is obvious that at 126K the spectrum of adsorbed CH_3CN has the same IR features as the spectrum of the bulk ice layer of CH_3CN but relative intensities differ. On warming this layer to 200K, the intensity of the symmetric $\upsilon(CH_3)$ mode is higher than that of the asymmetric $\upsilon(CH_3)$ mode while in the spectrum of the bulk ice layer of CH_3CN the reverse tendency appears. The 2251 cm^{-1} υ(CN) and its 2295 cm^{-1} Fermi resonance bands in the ice layer of CH_3CN have been replaced in the chemisorbed layer by two new bands at 2274 and 2303 cm^{-1}, which are assigned to the υ(CN) of the adsorbed CH_3CN and its Fermi resonance mode. The asymmetric υ(CH) mode moves to 1444 and 1414 cm^{-1} and the symmetric υ(CH) band moves to 1367 cm^{-1} for the chemisorbed species. The assignment of all IR bands is based on the liquid, solid, and gas-phase CH_3CN.[33,34] A comparison of the IR frequencies of CH_3CN in different states is given in Table 1.

Figure 2 shows a series of spectra in the υ(OH) region for adsorbed CH_3CN on TiO_2 at different temperatures. The broad band at ~3440 cm^{-1} corresponds to the associated OH groups on the surface while the bands at 3728, 3677, and 3608 cm^{-1} correspond to the different types of isolated OH groups on the surface.[35,36] The interaction between the adsorbed CH_3CN and the surface OH groups increases with increasing temperature above 126K as CH_3CN diffuses into the porous TiO_2 powder. The difference spectra of Figure 2 clearly show that with increasing temperature the intensity of the isolated OH bands decreases and that of the associated OH bands increases.

2. The Adsorption of CH_3CN on Different Types of TiO_2 Surfaces. Figure 3 shows the spectra of adsorbed CH_3CN on oxidized TiO_2 surfaces with different surface OH coverages. After initial treatment in a 6 Torr O_2 atmosphere, the TiO_2 was annealed in a vacuum at 1073K for 8 h to remove most of the surface OH groups. Then in a 50 Torr O_2 atmosphere, the TiO_2 was oxidized at 623K for 6 h and then cooled to room temperature, remaining at room temperature for 24 h before the O_2 was pumped out. The different surface OH coverages were obtained by admitting H_2O vapor into the IR cell. The left panel of Figure 3 shows the υ(OH) region while the right panel shows the υ(CN) region and its Fermi resonance mode. The 2318 cm^{-1} band disappeared when the surface was covered by a large amount of OH groups, which indicates that this band can be assigned to CH_3CN bonded to a surface Lewis acid site. The fact that the 2274 cm^{-1} band was observed only when surface OH groups were present implies that this band is due to the interaction between CH_3CN and surface OH groups, i.e., hydrogen-bonded CH_3CN.

TiO_2 can be made more defective by annealing in a vacuum. This process removes O^{2-} anions, leaving anion vacancy defect sites which are formally associated with Ti^{3+} ion centers, and surfaces produced in this manner are designated reduced TiO_2. The anion vacancy sites can be eliminated by reoxidation.[1] Figure 4 shows the spectra of adsorbed CH_3CN on the oxidized and reduced TiO_2 surfaces. The reduced TiO_2 surface was obtained by annealing the TiO_2 in a vacuum at 973K for 15 h while the oxidized TiO_2 surface was achieved by reoxidation and storage of the TiO_2 in 50 Torr of O_2. The υ(OH) region in the left panel clearly shows that almost the same coverage of OH groups was present on both oxidized and reduced TiO_2, indicating that the interaction between CH_3CN and surface OH

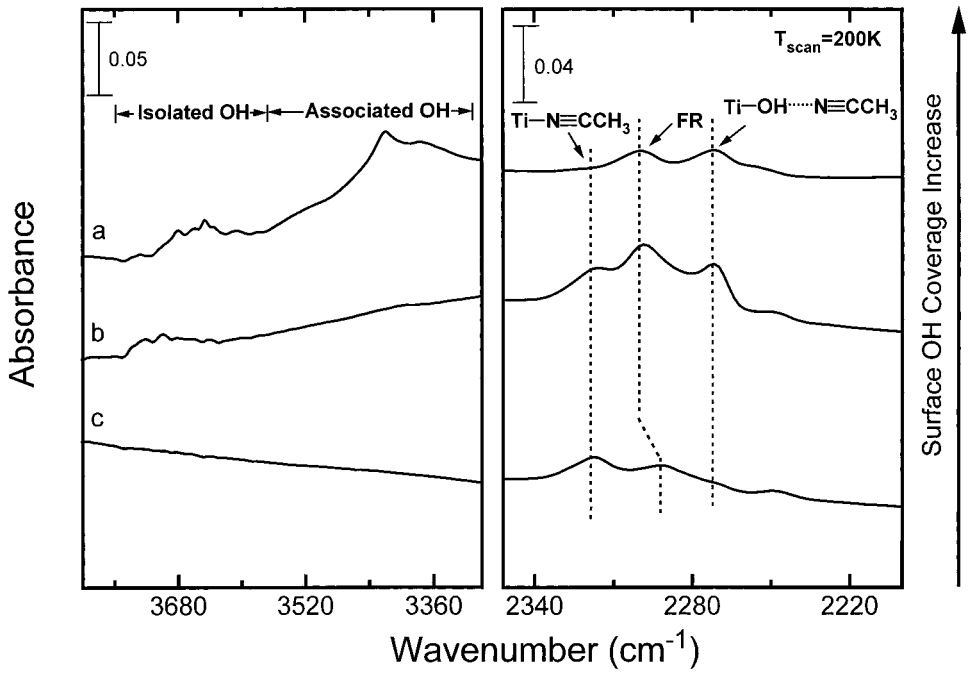

Figure 3. IR spectra in the region of υ(OH) and υ(CN) for CH_3CN adsorbed on TiO_2 with different OH coverages at 200 K, showing the hydroxyl and Lewis acid site bonded CH_3CN. FR represents the Fermi resonance mode of υ(CN). The TiO_2 was annealed at 1073K for 8 h and oxidized at 623 K for 6 h and 300 K for 24 h.

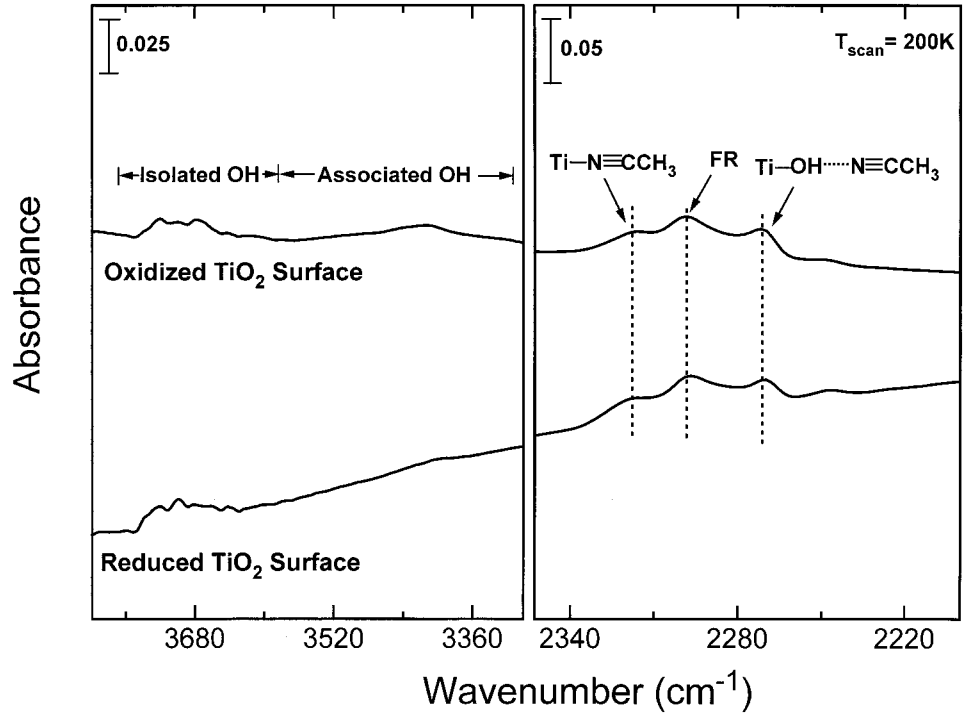

Figure 4. IR spectra in the region of υ(OH) and υ(CN) for CH_3CN adsorbed on the oxidized and reduced TiO_2 surface at 200 K, showing the lack of an effect of vacancy defect site production on the spectrum of chemisorbed CH_3CN. The TiO_2 was annealed at 973 K in a vacuum for 15 h to obtain a reduced surface. The oxidized surface was obtained by annealing at 973 K for 15 h then at 623 K for 6 h in 50 Torr O_2 and storage at 300 K for 24 h in 50 Torr O_2.

groups can be considered approximately equivalent. In the right panel three IR bands appear at 2318, 2298, and 2274 cm^{-1}, which can be assigned respectively to CH_3CN bonded to surface Lewis acid sites, to the Fermi resonance band, and to CH_3CN bonded to surface OH groups. The fact that on both oxidized and reduced TiO_2 surfaces the same three IR bands were observed proves that CH_3CN adsorbed on these two types of surfaces is undistinguishable. In other words, using IR spectroscopy, no difference is observed between CH_3CN adsorbed on TiO_2 containing Ti^{3+} defect sites,[37] and CH_3CN adsorbed on oxidized TiO_2 surfaces where the defect sites have been removed.

3. The Photooxidation of CH_3CN on TiO_2. *a. Products of the Photooxidation of CH_3CN.* The photooxidation of CH_3CN was carried out as follows: At 300K CH_3CN was adsorbed for 1 h on the TiO_2 surface which had been annealed at 973K for 15 h in advance. After the cell was evacuated, 50 Torr O_2 was introduced into the cell. During the UV irradiation of TiO_2, the

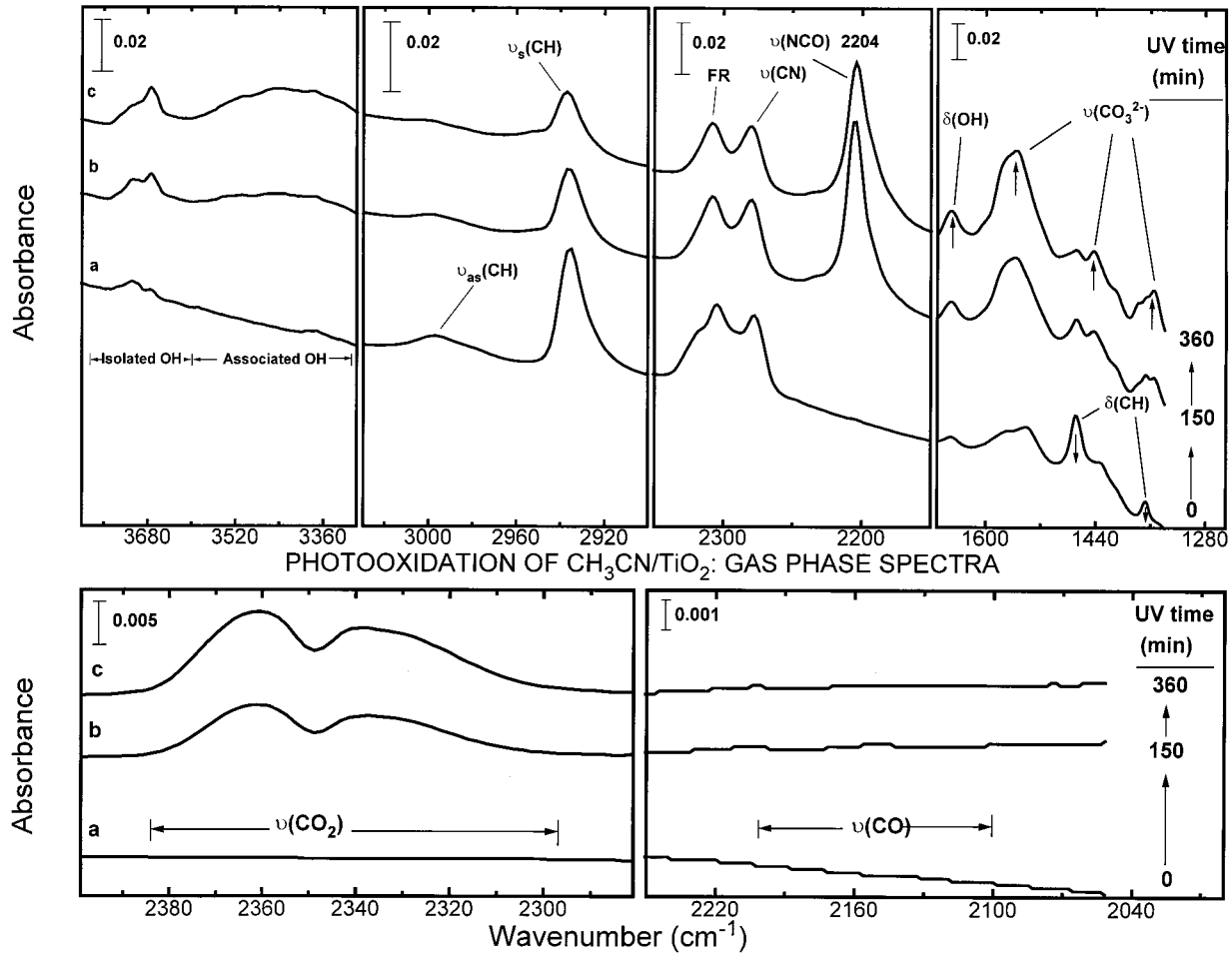

Figure 5. IR spectra of the surface species and gas-phase species formed during the photooxidation of CH_3CN with O_2 on the TiO_2 surface annealed at 973 K in a vacuum for 15 h as a function of UV exposure time at 305 K. The consumption of CH_3CN is observed by the decrease of intensity of the IR bands in the υ(CH) and the υ(CN) region. Surface OH, surface CO_3^{2-}, surface NCO species, and CO_2(g) are the observed products of the photoreaction.

course of the photooxidation of CH_3CN was continuously measured by IR measurements. The increase in temperature of the TiO_2 was less than 6K. Figure 5 shows a series of IR spectra for increasing of UV exposure time. The spectra of surface species and gas-phase species are shown in selected regions. Figure 5a is the IR spectrum before irradiation of TiO_2 by UV light. The spectrum of surface species shows the features of adsorbed CH_3CN on TiO_2 at 300K, which are characterized by the 2997 cm^{-1} asymmetric υ(CH) mode and the 2935 cm^{-1} symmetric υ(CH) mode, the 2277 cm^{-1} υ(CN) mode and its 2304 cm^{-1} Fermi resonance, the 1469 cm^{-1} asymmetric δ(CH) mode and the 1367 cm^{-1} symmetric δ(CH) band. The spectrum of the gas-phase species indicates that neither CO_2 nor CO was present inside the cell before UV irradiation.

After 5 min of exposure of the TiO_2 to the UV light, dramatic changes in the IR spectra of both the surface and the gas phase were observed. In the υ(CH) region of the surface spectra of Figure 5, the intensity of both the asymmetric 2977 cm^{-1} and symmetric 2935 cm^{-1} υ(CH) mode decreased as the function of the irradiation time. Also changes in the δ(CH) region show an intensity decrease of the asymmetric 1469 cm^{-1} δ(CH) mode and the symmetric 1367 cm^{-1} δ(CH) mode. This clearly shows that the adsorbed CH_3CN was photooxidated and consumed when the surface was irradiated by UV light in the presence of O_2(g). This conclusion can be further confirmed by the fact that in the υ(CN) region, the 2277 cm^{-1} υ(CN) mode and its 2304 cm^{-1} Fermi resonance mode also decreased as the UV irradiation time increased.

In the υ(OH) region of the surface spectra, two sharp IR bands at 3708 cm^{-1} and 3674 cm^{-1} and one broad IR band at ~3386 cm^{-1} were found to develop and increase in intensity with increasing UV exposure time. These IR features are assigned to the stretching modes of isolated surface OH groups and associated OH groups. The assignments for OH groups originally from the photoproduction of H_2O are in general agreement with the earlier studies.[36,38,39] Obviously this shows that water is one of the products formed during the photooxidation of CH_3CN on the TiO_2 surface.

In the $\upsilon(CO_2)$ region of the gas-phase spectra, the broad doublet at 2360 and 2337 cm^{-1}, due to CO_2 gas, was found to increase in intensity. Accompanying CO_2 production, peaks at 1556, 1442, and 1356 cm^{-1} in the $\upsilon(CO_3^{2-})$ region of the surface spectra also developed during the photoreaction and they are assigned to the surface carbonate or bicarbonate species formed from the reaction of the TiO_2 with CO_2 gas. The results obtained here are in general agreement with studies reported in the literature.[36,40,41] We did not observe the CO_2 surface species in the $\upsilon(CO_2)$ region of the surface spectra; CO_2 forms carbonate surface species in these experiments. No CO species were observed in the υ(CO) region for both the surface spectra and the gas-phase spectra.

An intense, sharp IR peak at 2204 cm^{-1} appeared in the υ(CN) region and developed with increasing UV exposure time. This band is assigned to the asymmetric υ(NCO) mode of the chemisorbed isocyanate species. The symmetric υ(NCO) mode is difficult to observe due to the heavy overlap with υ(CH) and

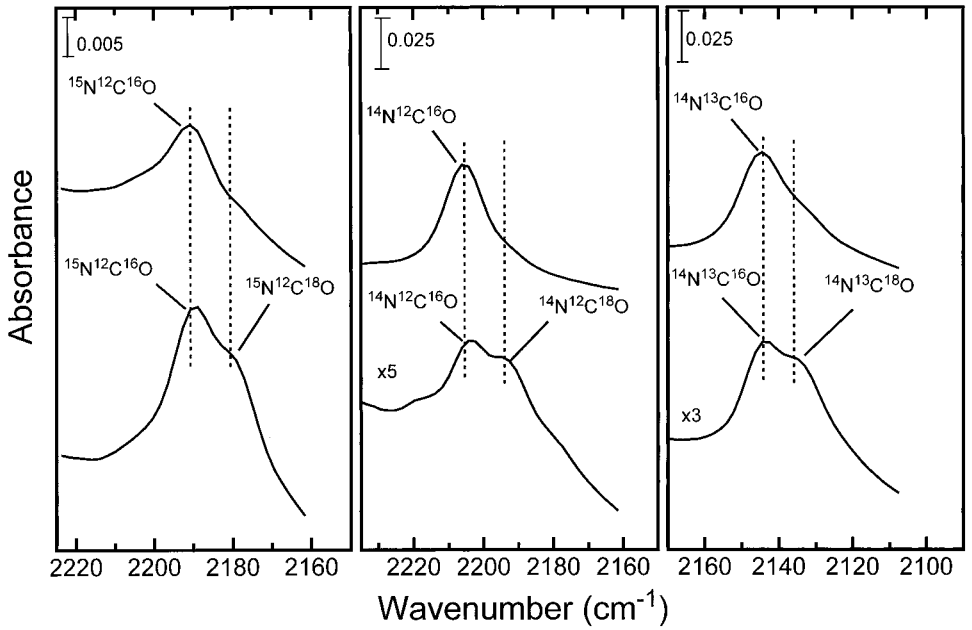

Figure 6. IR spectra in the υ(NCO) region during the photoreaction of CH_3CN, $CH_3{}^{13}CN$, and $CH_3C^{15}N$ with $^{16}O_2$ and $^{18}O_2$ on a 973 K annealed TiO_2 surface showing the isotopic NCO species produced. The spectra show that the surface species contains C, N, and O atoms.

$\upsilon(CO_3{}^{2-})$ modes in the same frequency region. The NCO assignment is supported by the isotopic shifts displayed in Figure 6. These spectra were obtained on the TiO_2 surface during the photooxidation of either $CH_3C^{15}N$ or $CH_3{}^{13}CN$ with either $^{16}O_2$ (shown in higher spectrum in each panel) or $^{18}O_2$ (shown in lower spectrum in each panel). The 2204 cm^{-1} peak shifted down to 2193 and 2144 cm^{-1} when the CH_3CN was substituted by the $CH_3C^{15}N$ and $CH_3{}^{13}CN$, respectively. When $^{18}O_2$ instead of $^{16}O_2$ was used, a shoulder whose frequency is 8−10 cm^{-1} lower than that of the corresponding ^{16}O peak appeared. The fact that the band shifts with ^{13}C, ^{15}N, and ^{18}O substitution clearly shows that this new species contains all three atoms. Further investigation of the assignment of the adsorbed isocyanate band will be discussed below.

b. Kinetics of the Photooxidation of CH_3CN on TiO_2. The kinetics plots in Figure 7 were obtained from the surface IR band intensities during the photooxidation of $CH_3C^{15}N$ on the TiO_2 surface. The combined integrated intensity of the 2254 cm^{-1} υ(CN) mode and its 2295 cm^{-1} Fermi resonance mode was used to monitor the consumption of CH_3CN while the intensity of the 2193 cm^{-1} υ(NCO) was monitored to determine the coverage change of the surface isocyanate species. Figure 7 clearly shows that the surface isocyanate species is an intermediate species, whose surface coverage passes through a maximum as photooxidation takes place. Two different slopes are seen in the kinetic curve for the consumption of CH_3CN, which implies that two different processes take place in the CH_3CN photooxidation. Two insets show the IR spectra in the υ(CN) region before UV irradiation (i.e., UV time equals 0 min) and after a 240 min UV irradiation. Two shoulders previously observed at ∼2301 cm^{-1} and ∼2260 cm^{-1} in the IR spectrum disappear after irradiation.

Figure 8 shows the kinetic plots for the formation of CO_2 gas (from the gas-phase spectra) during the photooxidation of $^{12}CH_3{}^{13}CN$ with $^{16}O_2$ on the TiO_2 surface. The inset is the gas-phase IR spectrum in the $\upsilon(CO_2)$ region after 150 min of UV irradiation. The $\upsilon(^{12}CO_2)$ doublet and $\upsilon(^{13}CO_2)$ doublet overlap each other. By comparing the pure $\upsilon(^{12}CO_2)$ spectrum and the pure $\upsilon(^{13}CO_2)$ spectrum, it is found that the overlap between $\upsilon(^{12}CO_2)$ and $\upsilon(^{13}CO_2)$ in the region above 2360 cm^{-1} and below 2372 cm^{-1} is negligible. The shaded area in the inset shows the integrated spectral region used to monitor the production of $^{12}CO_2$ and $^{13}CO_2$. From the kinetics plot, it is observed that the rate of formation of $^{13}CO_2$ exhibits an induction period which is not seen for $^{12}CO_2$. Therefore the ^{13}CN moiety in CH_3CN initially exhibits a diminished (or zero) rate of photooxidation compared to the $^{12}CH_3$ moiety.

Figure 9 shows the surface spectra for υ(NCO) for the photooxidation of CH_3CN with $^{18}O_2$ on the $Ti^{16}O_2$ surface during UV irradiation. Although the peaks of $\upsilon(NC^{16}O)$ and $\upsilon(NC^{18}O)$ are heavily overlapped, it is still obvious that the formation of the $NC^{16}O$ species is initially faster than that of the $NC^{18}O$ species, while at the end the $NC^{18}O$ species is formed faster than the $NC^{16}O$ species. This shows that photooxidation of CH_3CN adsorbed on TiO_2 involves lattice O from the TiO_2—an unusual finding.

4. Control Experiments. To determine whether CH_3CN is oxidized photochemically or thermally, CH_3CN was adsorbed on the TiO_2 surface and O_2 was admitted into the cell at 305K in the same manner as in the photooxidation experiments, but without UV irradiation. The upper spectra of Figure 10 show that no change was observed in the υ(CH), υ(CN), υ(NCO), $\upsilon(CO_3{}^{2-})$, and δ(CH) regions after 30 min, which indicates that the oxidation of CH_3CN is not a thermal process at 305K. Thus our experiments have observed only photochemically initiated surface processes. A second control experiment was done to check whether O_2 gas is necessary for the CH_3CN oxidation. The lower spectra of Figure 10 show that no change was observed when a saturated coverage of CH_3CN on the TiO_2 surface was irradiated for 30 min without O_2 gas. This shows that the presence of O_2 gas is critical for the photooxidation of CH_3CN on the TiO_2 surface.

IV. Discussion

1. Adsorption of CH_3CN on TiO_2—Adsorption Site Selection. At 126 K, the adsorption of CH_3CN forms a mixed chemisorbed layer and a condensed multilayer on the TiO_2 surface. It is often observed that a thick multilayer of adsorbate, condensed on top of chemisorbed species, will reduce

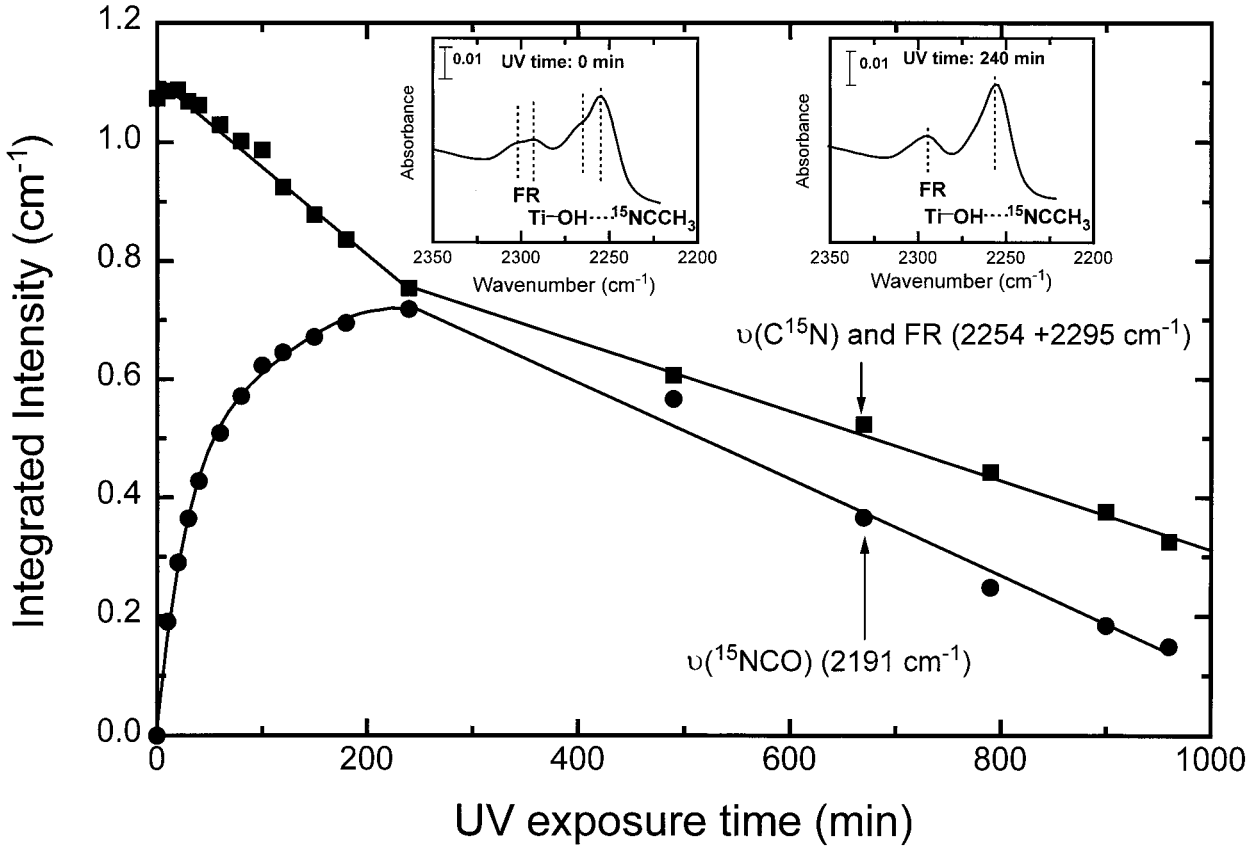

Figure 7. Surface kinetics plot of NCO and CH_3CN spectral intensity during the $CH_3C^{15}N$ photoreaction with O_2 on the TiO_2 surface. The two insets show the IR spectra in the region of υ(CN) before UV irradiation and after 240 min UV irradiation. FR represents the Fermi resonance mode.

TABLE 2: Comparison of υ(CN) of CH_3CN on Different Surfaces

CH_3CN species	surface	frequency (cm^{-1})	reference
$CH_3CN\cdots HO$	TiO_2	2274	this work
CH_3CN-Ti		2318	this work
$CH_3CN\cdots HO$	Al_2O_3	2253	29
CH_3CN-Al		2328	29
$CH_3CN\cdots HO^a$	zeolites	2278	26
CH_3CN-Al^b		2323	26
CH_3CN-Al^c		2332	26
$CH_3CN\cdots HO$	porous glass	2265	43
CH_3CN-Al		2345	43
CH_3CN-Zr		2292	43

[a] CH_3CN adsorbed on terminal SiOH group. [b] CH_3CN adsorbed on weak Lewis acid sites. [c] CH_3CN adsorbed on strong Lewis acid sites.

the IR intensity of the underlying species due to an optical screening effect. The incident E vector of the IR radiation is screened by the dielectric overlayer. This effect is clearly seen in Figure 1, spectrum a, for the Ti−OH mode. The same optical screening effect was observed when chemisorbed CO was covered by a condensed Xe layer on Ni(111).[42] With the increase in temperature, the disappearance of the features of the condensed layer and the development of intensity from the surface OH groups in Figure 1 (spectra b, c, and d) and Figure 2 indicate that the condensed CH_3CN multilayer diffuses into the porous TiO_2 powder. A schematic representation of this process is shown in Figure 11. The CH_3CN interacts with the surface OH groups to form the hydrogen-bonded surface CH_3CN species.

It is well known that the CN stretching frequency of CH_3CN at 2254 cm^{-1} shifts to higher frequency upon interaction with electron-accepting centers. In this study, the υ(CN) of CH_3CN adsorbed on the Bronsted and Lewis acid sites of the TiO_2 surface was found to shift to 2274 and 2318 cm^{-1} respectively. The CH_3CN molecules bonded to the Bronsted and Lewis acid sites of the TiO_2 surface are shown schematically below:

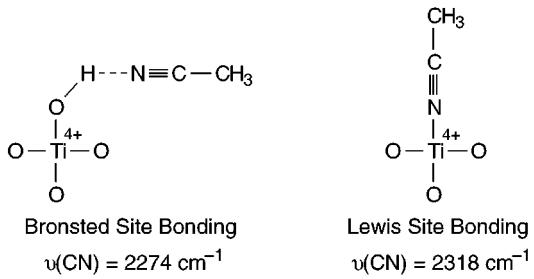

A comparison of υ(CN) of CH_3CN adsorbed on Bronsted and Lewis acid sites on different surfaces is given in Table 2.

It is surprising that the adsorption of CH_3CN on the annealed TiO_2 surface (containing anion vacancy defect sites) and on the oxidized surface yields the same IR spectra in the υ(CN) region. It is believed that Ti^{3+} sites are formed after annealing TiO_2 in a vacuum.[44] A stronger coordination complex between CH_3CN and Ti^{4+} sites on the oxidized surface compared to the complex between CH_3CN and Ti^{3+} sites on the annealed surface is expected. This should lead to a higher υ(CN) frequency for the surface $CH_3CN\cdots Ti^{4+}$ complex compared to the surface $CH_3CN\cdots Ti^{3+}$ complex. In homogeneous solutions the shift of the υ(CN) in CH_3CN upon coordination with $SnCl_4$, $AlCl_3$, and BF_3 was +51, +79, and +104 cm^{-1}, indicating that different coordination strength in the CH_3CN complex can lead to the different υ(CN) frequencies.[45] The υ(CN) of CH_3CN adsorbed on δ-θ alumina was found to be at 2328 cm^{-1} while on κ-alumina it was 2334 cm^{-1}.[46] A frequency shift has been found

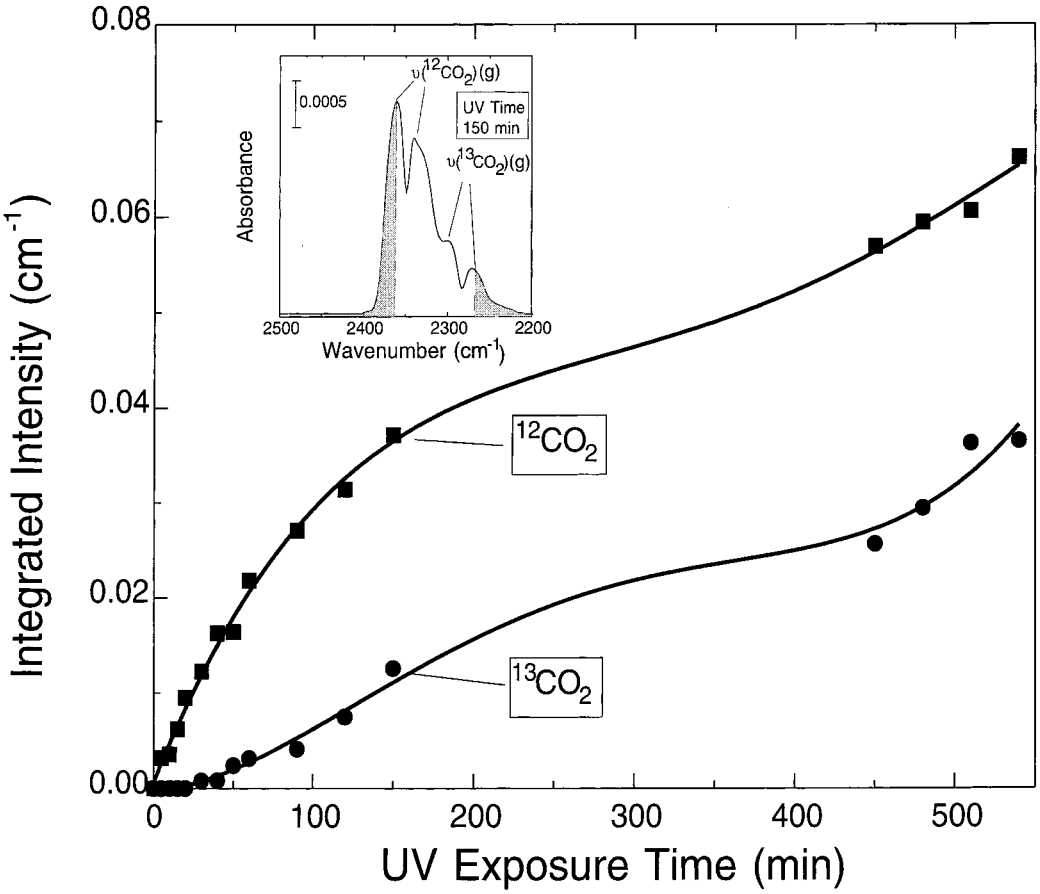

Figure 8. Gas-phase kinetics plot of the formation of CO_2 gas during the photooxidation of $CH_3{}^{13}CN$ with O_2 on the TiO_2 surface at 305 K. The inset shows the gas-phase IR spectrum in the $\upsilon(CO_2)$ region after 150 min UV irradiation.

between υ(CN) of $TiCl_3(CH_3CN)_3$ at 2280 cm^{-1} and υ(CN) of $TiCl_4(CH_3CN)_2$ at 2304 cm^{-1}.[47,48] The observed CH_3CN mode at 2318 cm^{-1} is consistent with CH_3CN bonding to Ti^{4+} sites on TiO_2. Possibly the Ti^{3+} sites are sterically unavailable to the CH_3CN molecule.

2. Photooxidation of CH_3CN on TiO_2. The products of the photooxidation of CH_3CN with O_2 on the TiO_2 surface observed by IR spectroscopy are H_2O, CO_2, and an intermediate surface NCO species. The ^{13}C, ^{15}N, and ^{18}O isotopic experiments in Figure 6 show that the 2204 cm^{-1} mode for $^{14}N^{12}C^{16}O$, observed in Figure 5, involves motion of all three atoms. Although a possible species coordinated to the surface Ti^{4+} could be the fulminate (Ti−CNO) species, the isocyanate (Ti−NCO) species is far more common. The C-bonded fulminate species (CNO) was found to be far less stable than the isocyanate species (NCO) on Ni(100) by an ab initio study.[49] The same study indicated that the linear NCO species bound through the N atom (isocyanate species) was more stable that either a linear NCO species bound through the O atom (cyanate species) or the side-on bonded NCO species on the surface.[49] In the study of cyanate and isocyanate surface species on Rh/SiO_2, the theoretical computations for RhNCO and RhOCN also predict the more stable isocyanate species, although only by 12.4 kcal/mol.[50] So it is likely that the surface NCO species is bonded through the N atom to a Ti^{4+} center. The same configuration of NCO on the Cu(100) surface was suggested in a recent study.[51] The magnitudes of the isotopic shifts seen in this study are very similar to the shifts observed for different NCO isotopomers on Cu(100) and on Ru(001).[51,52] A much bigger isotopic shift for $HC^{15}NO$ was observed in the IR study of HCNO, which further supports our assignment of NCO species.[53] An early study showed that a 2210 cm^{-1} mode was observed in the IR spectrum for adsorption of HNCO on the TiO_2 surface.[54] A similar υ(NCO) frequency has been observed for NCO adsorbed on the Cu(100) surface (2201 cm^{-1}),[51] on the Ni/SiO_2 surface-(2201 cm^{-1})[55] and on the Pt/TiO_2 surface (2210 cm^{-1}).[56] In the case of oxide-support metals, it is likely that the NCO species is present on the oxide surfaces. A comparison of υ(NCO) of NCO species on different surfaces is given in Table 3.

TABLE 3: Comparison of υ(NCO) of Different NCO Species

NCO species	surface	frequency (cm^{-1})	reference
Ti−NCO	TiO_2	2204	this work
Ti−NCO	TiO_2	2210	54
Ti−NCO	Pt/TiO_2	2210	56
Ti−NCO	Ag/TiO_2	2204	57
Cu−NCO	Cu(100)	2201	51
Ni−NCO	Ni/SiO_2	2201	55
Al−NCO	Al_2O_3	2258	58
Ag−NCO	Ag/Al_2O_3	2235	58

Although Figure 7 clearly indicates the surface NCO species is a reaction intermediate, the final N-containing product was not observed in the IR spectrum. The possible explanation is that the final N-containing product is not an IR-active species. The products of the photolysis of the HNCO gas were found to be CO, H_2, and N_2.[59] In the presence of O_2, the complete suppression of H_2 formation was observed while the yields of CO and N_2 was unchanged.[60] Therefore it is likely that the surface NCO species went through a similar process during UV irradiation forming N_2 and CO in the presence of O_2. The CO was immediately oxidized by O_2 to produce CO_2 gas. The formation of the $^{13}CO_2$ gas from the photooxidation of

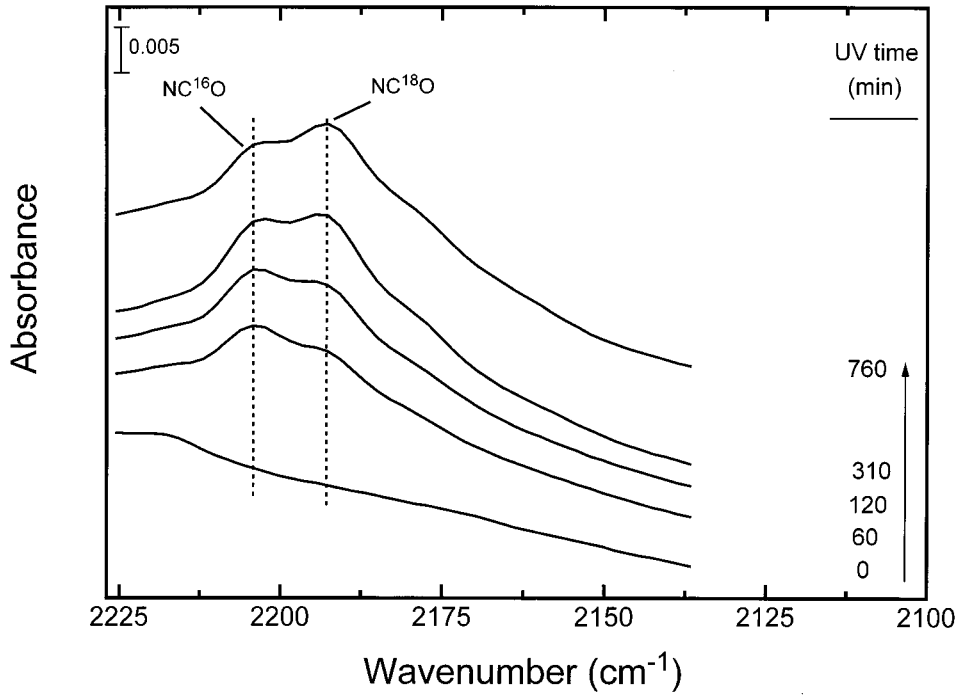

Figure 9. IR spectra of surface $NC^{16}O$ and $NC^{18}O$ species formed during the photoreaction of CD_3CN with $^{18}O_2$ on TiO_2, annealed at 973 K for 15 h, as a function of UV exposure time.

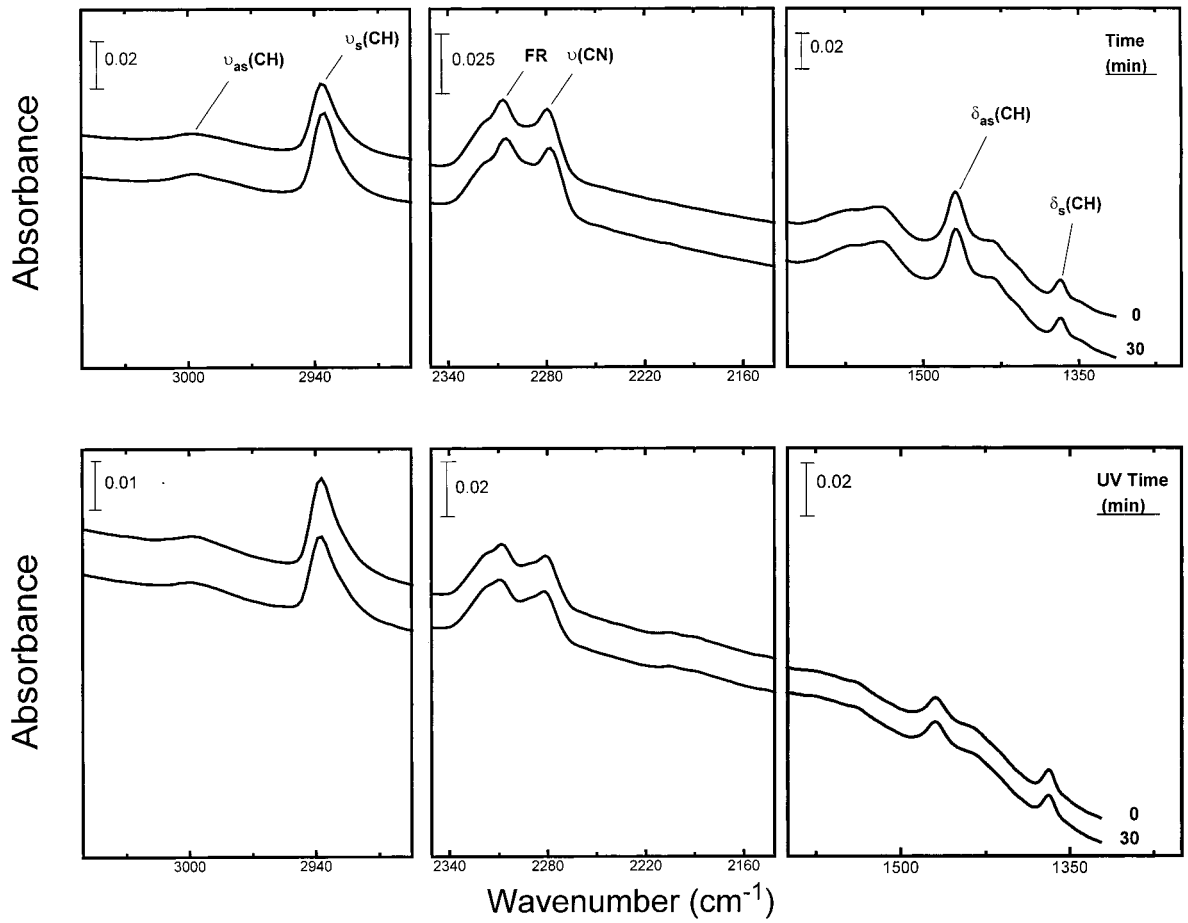

Figure 10. IR spectra of two control experiments as a function of time. The spectra show that neither the thermal reaction of CH_3CN with O_2 on TiO_2 at 305 K (top) nor the photoreaction of CH_3CN on TiO_2 without O_2 gas occurs (bottom).

$^{12}CH_3{}^{13}CN$ on the TiO_2 surface, shown in the inset of Figure 8, supports the above discussion. In the recent study by Lichtin et al., instead of NCO, $(CN)_2$ and NO_2 were observed as the intermediates in the photooxidation of CH_3CN on the TiO_2 surface and HNO_3 was identified as a final product.[30] But the study by Celio et al. shows that at 300K, the $(CN)_2$ can be oxidized to the isocyanate in the presence of O_2 gas on a Cu(100) surface.[51] Therefore it is possible that the $(CN)_2$ observed by Lichtin et

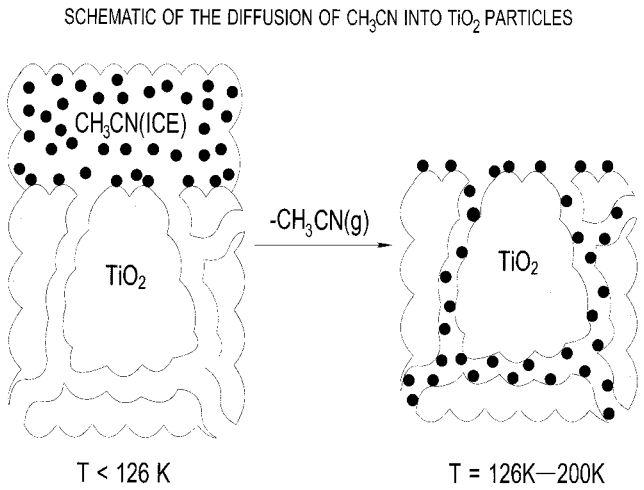

Figure 11. Schematic of the diffusion of CH_3CN into TiO_2 particles with increasing temperature.

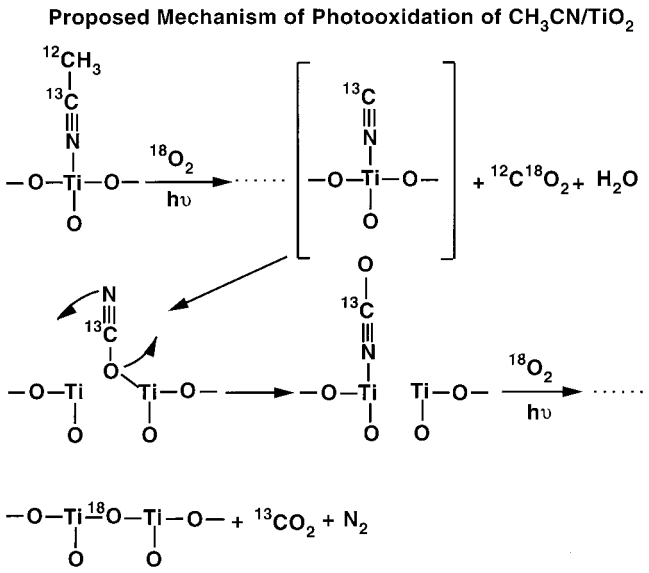

Figure 12. Schematic of the proposed mechanism of CH_3CN photooxidation on TiO_2.

al. was oxidized to the surface isocyanate species in our study and then went through a different oxidation sequence.

No CO was detected in the photooxidation of CH_3CN in both the surface IR spectrum and the gas-phase IR spectrum. The previous studies of photooxidation of CH_3Cl and TCE on TiO_2 showed the existence of CO as an intermediate in both the surface and the gas-phase spectrum.[21,22] Due to the high pressure of O_2 in this study (50 Torr), the reaction rate from CO to CO_2 could be so fast that the concentration of CO(g) was too low to be seen by IR spectroscopy. CO adsorption on the $TiO_2(110)$ surface occurs at in-plane Ti sites on both oxidized and reduced surfaces.[61]

The TiO_2 used in this study is highly dehydroxylated after the 973K activation for 15 h before the photooxidation experiment. Only a small coverage of OH groups is initially present on the surface, which can be seen in the surface IR spectra of Figure 5 (spectrum a). This fact indicates that adsorbed water is not necessary for the onset of the photooxidation of CH_3CN on the TiO_2 surface. Indeed, surface OH groups are produced from the photooxidation of CH_3CN on TiO_2 as seen in Figure 5 (spectra b and c). The photooxidation rate of CH_3CN on the TiO_2 surface has been observed to decrease with increasing concentration of water vapor.[30] On the other hand, the control experiment involving UV irradiation of adsorbed CH_3CN on the TiO_2 surface without O_2 gas (Figure 10) shows that CH_3CN cannot be oxidized in the absence of O_2 gas. This indicates that O_2 gas is an indispensable reactant for the photooxidation of CH_3CN, implying that the function of O_2 is not just that of an electron scavenger.

3. Mechanism for the Photooxidation of CH_3CN on TiO_2. The experimental results presented here are not sufficient for us to postulate a complete mechanism for the photooxidation of CH_3CN on the TiO_2 surface.

The photooxidation experiment of CD_3CN with $^{18}O_2$ on the $Ti^{16}O_2$ surface show that not only $NC^{18}O$ but also $NC^{16}O$ were formed on the surface. This proves definitely that the lattice O atom is involved in the photoreaction since it is the only source of ^{16}O atoms. Furthermore, the $NC^{16}O$ surface species was formed faster than the $NC^{18}O$ species at the beginning of photoreaction.

Figure 12 schematically indicates how the formation of adsorbed NCO species may occur by photooxidation of adsorbed CH_3CN. This process involves adsorbed O_2, yet still preferentially incorporates lattice O species into NCO. The mechanism indicates that the CH_3 moiety of adsorbed CH_3CN is first oxidized by attack of electronically excited adsorbed O_2. The mechanism of this step is not understood at present. However, an adsorbed CN radical produced and this radical species is active for attack of TiO_2 forming NCO species by insertion of the carbon moiety into a Ti−O bond yielding the Ti−OCN species which then inverts to the Ti−NCO species which is detected spectroscopically as a surface intermediate. A subsequent photooxidation step converts Ti−NCO to the final oxidation products, CO_2 (CO_3^{2-}), and N_2 (not observed in these experiments). The production of Ti−NCO with lattice O results in the formation of O-lattice vacancies. When $^{18}O_2(g)$ is present, $^{18}O_2$ is dissociatively adsorbed or is photochemically dissociated at these sites,[1] producing an ^{18}O labeled Ti−O site on the TiO_2 surface. Ultimately, complete labeling of the TiO_2 surface with ^{18}O results in increased formation of the $Ti-NC^{18}O$ intermediate species (see Figure 9) and then $C^{18}O_2(g)$.

This two step mechanism involving initially the photooxidation of the CH_3 moiety in adsorbed CH_3CN is supported by the observation that CO_2 originally from the CH_3 group is first observed (Figure 8). CO_2 originating from the CN moiety of CH_3CN is delayed in its production. The observed NCO intermediate, leading to the final oxidation of the CN moiety, exhibits the kinetic behavior expected for an intermediate species (Figure 7).

The two different kinetic processes for the consumption of $CH_3C^{15}N$ on the TiO_2 surface are indicated by the two different slopes of the kinetics plot of Figure 7. The two insets in Figure 7 show that before the UV irradiation two shoulders are present in the υ(CN) peak of adsorbed CH_3CN and its Fermi resonance peak, while after 240 min of irradiation the two shoulders disappear. Correspondingly, after 240 min of irradiation, the rate of loss of intensity of υ(CN) and its Fermi resonance decreases. This implies that CH_3CN is adsorbed on two different surface sites. These two CH_3CN species exhibit different kinetics during photoreaction. The more strongly bonded CH_3CN species exhibits faster photooxidation kinetics.

V. Conclusions

The adsorption of CH_3CN and its photooxidation with O_2 on a powdered TiO_2 surface was investigated by transmission

infrared spectroscopy at 305K. The following conclusions have been obtained.

(1) A chemisorbed layer and a physisorbed ice layer are formed upon the adsorption of CH_3CN on TiO_2 at 126K. With increasing temperature, diffusion of CH_3CN into the porous TiO_2 occurs, forming chemisorbed CH_3CN at surface OH (Bronsted) sites.

(2) The adsorption of CH_3CN on surface Lewis acid sites has also been spectroscopically observed.

(3) The photooxidation of CH_3CN on TiO_2 produces H_2O (observed as surface OH groups), CO_2, surface CO_3^{2-}, and an adsorbed NCO species, which is identified as an intermediate.

(4) The presence of O_2 gas is necessary for the photooxidation of CH_3CN on by TiO_2 surface while water or surface OH groups are not.

(5) Two different photooxidation kinetic processes in the photooxidation of CH_3CN on the TiO_2 surface were observed and are postulated to be related to the adsorption of CH_3CN on different surface sites.

(6) The photooxidation chemistry consists of two overall kinetic steps. In the first step, the CH_3 moiety of adsorbed CH_3CN is preferentially photooxidized, liberating a CN radical species. The CN radical species attacks Ti−O bonds in the TiO_2 surface to produce Ti−NCO species which are observed as an intermediate surface species. Ti−NCO species are then further oxidized to CO_2 (CO_3^{2-}) and to N_2 (not observed in these experiments).

(7) The experiment indicates that stepwise photooxidation of multifunctional molecules may occur on TiO_2, and that while O_2 gas is essential, a subsequent process involving lattice O from TiO_2 is also of importance.

Acknowledgment. We thank the Army Research Office for support of this work.

References and Notes

(1) Linsebiger, A.; Lu, G.; Yates, J. T. Jr. *Chem. Rev*. **1995**, *95*, 735.
(2) Kamat, P. V. *Chem. Rev.* **1993**, *93*, 267.
(3) Fox, M. A.; Dulay, M. T. *Chem. Rev.* **1993**, *93*, 341.
(4) Hoffmann, M. R.; Martin, S. T.; Wonyong, C.; Bahnemann, D. W. *Chem. Rev.* **1995**, *95*, 69.
(5) Nimlos, M. R.; Jacoby, W. A.; Blake, D. M.; Milne, T. A. *Environ. Sci. Technol.* **1993**, *27*, 732.
(6) Glaze, W. H.; Kenneke, J. F.; Ferrry, J. L. *Environ. Sci. Technol.* **1993**, *27*, 177.
(7) Luo, Y.; Ollis, D. F. *J. Catal*. **1996**, *163*, 1.
(8) Stafford, U.; Gray, K. A.; Kamat, P. V.; Varma, A. *Chem. Phys. Lett.* **1993**, *205*, 55.
(9) Lu, G.; Linsebigler, A.; Yates, J. T., Jr. *J. Chem. Phys.* **1995**, *99*, 7626.
(10) Fox, M. A. In *Photocatalytic Purification and Treatment of Water and Air*; Ollis, D. F., Al-Ekabi, H.; Elsevier: Amsterdam, The Netherlands 1993; p 163.
(11) Brezova, V.; Stasko, A. *J. Catal*. **1994**, *147*, 156.
(12) Nada., H.; Oikawa, K.; Ohya-Nishiguchi, H.; Kamada, H. *Bull. Chem. Soc. Jpn.* **1994**, *67*, 2301.
(13) Milles, G.; Hoffman, M. R. *Environ. Sci. Technol.* **1993**, *27*, 1681.
(14) Wei, T. Y.; Wan, C. *J. Photochem. Photobiol., A* **1992**, *69*, 241.
(15) Mills, A.; Morris, S.; Davies, R. *J. Photochem. Photobiol., A* **1993**, *70*, 183.
(16) Goldstein, S.; Czapski, G.; Rabani, J. *J. Phys. Chem.* **1994**, *98*, 6586.
(17) Micic, O. I.; Zhang, Y.; Cromack, K. R.; Trifunac, A. D.; Thurnauer, M. C. *J. Phys. Chem.* **1993**, *97*, 7277.
(18) Nakakoa, Y.; Nosaka, Y. *J. Photochem. Photobiol., A* **1997**, *110*, 299.
(19) Jones, A. P.; Watts, R. J. *J. Environ. Eng.* **1997**, *123*, 974.
(20) Cunningham, J.; Srijarana, S. *J. Photochem. Photobiol., A* **1988**, *43*, 329.
(21) Wong, J. C. S.; Linsebigler, A.; Lu, G.; Fan, J.; Yates, J. T., Jr. *J. Phys. Chem.* **1995**, *99*, 335.
(22) Fan, J.; Yates, J. T., Jr. *J. Am. Chem. Soc.* **1996**, *118*, 4686.
(23) Okamoto, K.; Yamamoto, Y.; Tanaka, H.; Tanaka, M. *Bull. Chem. Soc. Jpn.* **1985**, *58*, 2015.
(24) Angell, C. L.; Howell, M. V. *J. Phys. Chem.* **1969**, *73*, 2551.
(25) Sempels, R. E.; Rouxhet, P. G. *J. Colloid. Interface Sci.* **1976**, *55*, 263.
(26) Pelmenschikov, A. G.; van Santen, R. A.; Janchen, J.; Meijer, E. *J. Phys. Chem.* **1993**, *97*, 11071.
(27) Aboulayt, A.; Binet, C.; Lavalley, J. C. *J. Chem. Soc., Faraday Trans.* **1995**, *91*, 2913.
(28) Hagiwara, K.; Yamazaki, T.; Ozawa, S. *J. Colloid Interface Sci.* **1995**, *170*, 421.
(29) Knözinger, H.; Krietenbrink, H. *J. Chem. Soc., Faraday Trans. 1* **1975**, *71*, 2421.
(30) Lichtin, N. N.; Avudaithai, M. *Environ. Sci. Technol.* **1996**, *30*, 2014.
(31) Basu, P.; Ballinger, T. H.; Yates, J. T., Jr. *Rev. Sci. Instrum.* **1988**, *59*, 1321.
(32) Muha, R. J.; Gates, S. M.; Yates, J. T., Jr.; Basu, P. *Rev. Sci. Instrum.* **1985**, *56*, 613.
(33) Pace, E. L.; Noe, L. J. *J. Chem. Phys.* **1968**, *49*, 5317
(34) Parker, F. W.; Nielsen, A. H.; Fletcher, W. H. *J. Mol. Spectrosc.* **1957**, *1*, 107
(35) Smith, I. T. *Nature* **1964**, *201*, 67.
(36) Yates, D. J. C. *J. Phys. Chem.* **1961**, *65*, 746.
(37) Lu, G.; Linsebigler, A.; Yates, J. T., Jr. *J. Phys. Chem*. **1994**, *98*, 11733.
(38) Primet, M.; Pichat, P.; Mathieu, M. V. *J. Phys. Chem.* **1971**, *75*, 1216.
(39) Tanaka, K.; White, J. M. *J. Phys. Chem.* **1982**, *86*, 4708.
(40) Jackson, P.; Parfitt, G. D. *J. Chem. Soc., Faraday Trans. 1* **1972**, *68*, 896.
(41) Morterra, C.; Chiorino, A.; Boccuzzi, F. *Z. Phys. Chem. (Munich)* **1981**, *124*, 211.
(42) Xu, Z.; Sherman, M. G.; Yates, J. T., Jr.; Antoniewicz, P. R. *Surf. Sci.* **1992**, *276*, 249.
(43) Low, M. J. D.; Bartner, P. L. *Can. J. Chem.* **1970**, *48*, 7.
(44) Göpel, W.; Rocker, G.; Feierabend, R. *Phys. Rev. B* **1983**, *28*, 3427.
(45) Purcell, K. F.; Drago, R. S. *J. Am. Chem. Soc.* **1966**, *88*, 919.
(46) Healy, M. H.; Wieserman, L. F.; Arnett, E. M.; Wefers, K. *Langmuir* **1995**, *5*, 114.
(47) Duckworth, M. W.; Fowles, G. W. A.; Hoodless, R. A. *J. Chem. Soc., Faraday Trans.* **1963**, *59*, 5665.
(48) Coerver, H. J.; Curran, C. *J. Am. Chem. Soc.* **1958**, *80*, 3522.
(49) Yang, H.; Whitten, J. L. *Surf. Sci*. **1998**, *401*, 312.
(50) Paul, D. K.; Mckee, M. L.; Worley, S. D.; Hoffman, N. W.; Ash, D. H.; Gautney, J. *J. Phys. Chem.* **1989**, *93*, 4598.
(51) Celio, H.; Mudalige, K.; Millis, P.; Trenary, M. *Surf. Sci.* **1997**, *394*, L168.
(52) Jakob, P. *Chem. Phys. Lett.* **1996**, *263*, 607.
(53) Quapp, W.; Albert, S.; Winnewisser, B. P.; Winnewisser, M. *J. Mol. Spectrosc*. **1993**, *160*, 540.
(54) Solymosi, F.; Bansagl, T. *J. Am. Chem. Soc.* **1979**, *83*, 552.
(55) Morrow, B. A.; Sont, W. N.; Onge, A. S. *J. Catal*. **1980**, *62*, 304.
(56) Solymosi, F.; Volygesi, L.; Sarkany, J. *J. Catal*. **1978**, *54*, 336.
(57) Kameoka, S.; Chafik, T.; Ukisu, Y.; Miyadera, T. *Catal. Lett.* **1998**, *51*, 11
(58) Kameoka, S.; Chafik, T.; Ukisu, Y.; Miyadera, T. *Catal. Lett.* **1998**, *55*, 211
(59) Mui, J. Y. P.; Back, R. A. *Can. J. Chem.* **1963**, *41*, 826.
(60) Back, R. A.; Ketcheson, R. *Can. J. Chem.* **1968**, *46*, 531.
(61) Linsebigler, A.; Lu, G.; Yates, J. T., Jr. *J. Phys. Chem.* **1996**, *100*, 6631